Received: 11 April 2019 | Revised: 30 June 2019 | Accepted: 1 July 2019

DOI: 10.1002/pro.3675

ARTICLE

THE PROTEIN SOCIETY WILEY

Structural and functional studies of USP20 ZnF-UBP domain by NMR

Yuanyuan Yang[1,2] | **Yiluan Ding**[1] | **Chen Zhou**[1] | **Yi Wen**[3] | **Naixia Zhang**[1,2]

[1]Department of Analytical Chemistry, Shanghai Institute of Materia Medica Chinese Academy of Sciences, Shanghai, China

[2]University of the Chinese Academy of Sciences, Beijing, China

[3]Oxford Instruments Technology (Shanghai) Co., Ltd, Shanghai, China

Correspondence
Naixia Zhang, Department of Analytical Chemistry, Shanghai Institute of Materia Medica Chinese Academy of Sciences, 555 Zu Chong Zhi Road, Shanghai 201203, China.
Email: nxzhang@simm.ac.cn

Funding information
National Natural Science Foundation of China, Grant/Award Number: 21778061; National Science & Technology Major Project "Key New Drug Creation and Manufacturing Program" of China, Grant/Award Number: 2018ZX09711002

Abstract

Deubiquitinase USP20/VDU2 has been demonstrated to play important roles in multiple cellular processes by controlling the life span of substrate proteins including hypoxia-inducible factor HIF1α, and so forth. USP20 contains four distinct structural domains including the N-terminal zinc-finger ubiquitin binding domain (ZnF-UBP), the catalytic domain (USP domain), and two tandem DUSP domains, and none of the structures for these four domains has been solved. Meanwhile, except for the ZnF-UBP domain, the biological functions for USP20's catalytic domain and tandem DUSP domains have been at least partially clarified. Here in this study, we determined the solution structure of USP20 ZnF-UBP domain and investigated its binding properties with mono-ubiquitin and poly-ubiquitin (K48-linked di-ubiquitin) by using NMR and molecular modeling techniques. USP20's ZnF-UBP domain forms a spherically shaped fold consisting of a central β-sheet with either one α-helix or two α-helices packed on each side of the sheet. However, although having formed a canonical core structure essential for ubiquitin recognition, USP20 ZnF-UBP presents weak ubiquitin binding capacity. The structural basis for understanding USP20 ZnF-UBP's ubiquitin binding capacity was revealed by NMR data-driven docking. Although the electrostatic interactions between D264 of USP5 (E87 in USP20 ZnF-UBP) and R74 of ubiquitin are kept, the loss of the extensive interactions formed between ubiquitin's di-glycine motif and the conserved and non-conserved residues of USP20 ZnF-UBP domain (W41, E55, and Y84) causes a significant decrease in its binding affinity to ubiquitin. Our findings indicate that USP20 ZnF-UBP domain might have a physiological role unrelated to its ubiquitin binding capacity.

KEYWORDS

deubiquitinase, NMR, solution structure, USP20, ZnF-UBP domain

1 | INTRODUCTION

Ubiquitination is a reversible protein posttranslational modification, which has been revealed to play pivotal roles in multiple cellular processes including protein degradation, protein trafficking, DNA repair, signal transduction, and so forth.[1–3] Ubiquitination is catalyzed by an enzymatic cascade composed of ubiquitin-activating enzyme (E1), ubiquitin-conjugating enzyme (E2), and ubiquitin ligase (E3). Meanwhile, the reverse process of ubiquitination (deubiquitination) is promoted by deubiquitinase (DUB). These enzymes are key players of protein ubiquitination and deubiquitination system, which display their activities by regulating the life span, the subcellular localization, and the activation–deactivation of

substrate proteins.[4–7] There are a total number of 1–2 E1s, tens of E2s, hundreds of E3s, and ~100 DUBs in eukaryotes.[8–10] The E3 ligases and the DUBs play fundamental roles in conferring specificities toward substrate proteins and the ubiquitin chain linkages built on them.[11] According to the functional and the structural similarities, DUBs are divided into six subfamilies which include the ubiquitin-specific proteases (USPs), the ubiquitin carboxy-terminal hydrolases (UCHs), the ovarian-tumor proteases (OTUs), the Machado-Joseph disease protein domain proteases (MJDs), the JAMM/MPN domain-associated metallopeptidases (JAMMs), and the motif-interacting with ubiquitin-containing novel DUBs (MINDYs).[12–14] More than 50% of the DUBs belong to USP subfamily, all of which contain a conserved USP catalytic domain surrounded by one or more additional domains.[5,11,13]

USP20 belongs to the USP subfamily of DUBs. It is involved in multiple cellular processes by controlling the lifespan of hypoxia-inducible factor HIF1α, Type 2 iodothyronine deiodinase (D2), β1/β2-adrenergic receptor, Tax, tumor necrosis factor receptor-associated factor 6, pyruvate kinase isoenzyme M2, and β-catenin.[15–24] USP20 is a potential target for antitumor drug development. Inhibition of USP20 might downregulate the deubiquitination of HIF1α, and prevents its proteasomal degradation and the following transcription of hypoxic response genes. Currently, there is one inhibitor of USP20 in preclinical stage developed by the GlaxoSmithKline has been reported.[7] Human USP20 consists of 914 amino acids and contains four distinct structural domains including the N-terminal ZnF-UBP domain, the USP catalytic domain, and two tandem DUSP domains. The ZnF-UBP domain is a small ubiquitin binding module characterized by coordinated zinc ions and ubiquitin binding capacity. It has been found in a few of USP DUB family members (USP5, USP13, USP16, USP20, USP33, etc.), the ubiquitin ligase IMP/BRAP2, and the deacetylase HDAC6.[25–27] The structural and functional properties of ZnF-UBP domain in USP5 (also named as IsoT) have been well studied. The crystal structure of USP5 ZnF-UBP/ubiquitin complex has revealed the structural basis for the recognition and binding of free ubiquitin C-terminal diglycine motif by USP5 ZnF-UBP hydrophobic pocket.[28] In addition, the previously reported study of USP33 indicates that the USP33 ZnF-UBP domain, as well as USP20 ZnF-UBP domain, probably could not recognize ubiquitin.[29] Here in this article, by a combined use of NMR and molecular modeling techniques, the solution structure of USP20 ZnF-UBP domain was solved, and its ubiquitin binding capacity was characterized. The achieved data suggest that although USP20 ZnF-UBP domain forms a canonical ubiquitin binding fold, its binding affinities with mono-ubiquitin and ubiquitin chain (K48-linked di-ubiquitin) are quite weak. The structural basis for understanding USP20 ZnF-UBP's weak ubiquitin binding capacity was revealed by the model structures of USP20 ZnF-UBP/K48-linked di-ubiquitin complexes determined by the NMR data-driven docking. The substitutions of residue R221 in USP5 ZnF-UBP to E55 in USP20 ZnF-UBP abolishes the extensive interactions between this residue and the free C-terminus diglycine motif of ubiquitin, and cause a significant decrease in the binding affinity of USP20 ZnF-UBP to ubiquitin. The results obtained in this research suggest that USP20 ZnF-UBP might have a different physiological role from those ZnF-UBP domains with strong binding affinities to ubiquitin.

2 | RESULTS

2.1 | Structure determination of USP20 ZnF-UBP domain

The ZnF-UBP domain is a small conserved module found in many proteins in the ubiquitin system (Figure 1a). To investigate the structural basis for functional display of USP20 ZnF-UBP domain, we initially purified the USP20 ZnF-UBP domain and determined its solution structure by using NMR techniques. The calculation results and structural statistics of the 20 lowest-energy structures are summarized in Table 1. As that shown in Figure 1b, USP20 ZnF-UBP domain forms a well folded structure in spherical shape that composed of three α-helices and five β-strands in a ααββαββββ sandwich arrangement. The core structure of USP20 ZnF-UBP domain is the five antiparallel β-strands, which locates at the center in an order of β2-β1-β3-β4-β5, and surrounded by three α-helices with α1 and α2 packing on one side while α3 on the other side. The overall construction of USP20 ZnF-UBP domain is stabilized by three tetrahedrally coordinated zinc ions. Two of them adopt a C3H coordination pattern (Zn1: C8, H10, C83, C86; Zn2: C30, C33, C53, H60; Figure 1c) and the other one was coordinated in the form of C2H2 (Zn3: C43, C48, H64, H70; Figure 1c).

According to the published structures of ZnF-UBP domains in different USPs (USP5, USP13, USP33, USP16), the central antiparallel β-sheet and the particular α-helix between β2 and β3 (α3 in USP20 ZnF-UBP domain) are highly conserved.[28–31] The unique structural features for each ZnF-UBP domain from different USPs embody in the structural variations in the non-conserved α-helices, loop regions, and zinc coordination patterns. The particular residues locating at the central β-sheet and the loop between β2 and α3 (named L2A in the USP5 ZnF-UBP domain structure) gather together spatially and form a typical ubiquitin binding pocket.

The ZnF-UBP domain of USP33, which is the homologue of USP20, forms an identical ααββαββββ global fold and also the same zinc ion coordination pattern as USP20 ZnF-UBP domain (Figure 2a). The structural differences of these two ZnF-UBP domains are mainly from the flexible loops, especially the loop between β2 and α3 (loop L2A), which has been reported to play a critical role in ubiquitin recognition. In addition, the surface charge distribution of USP20

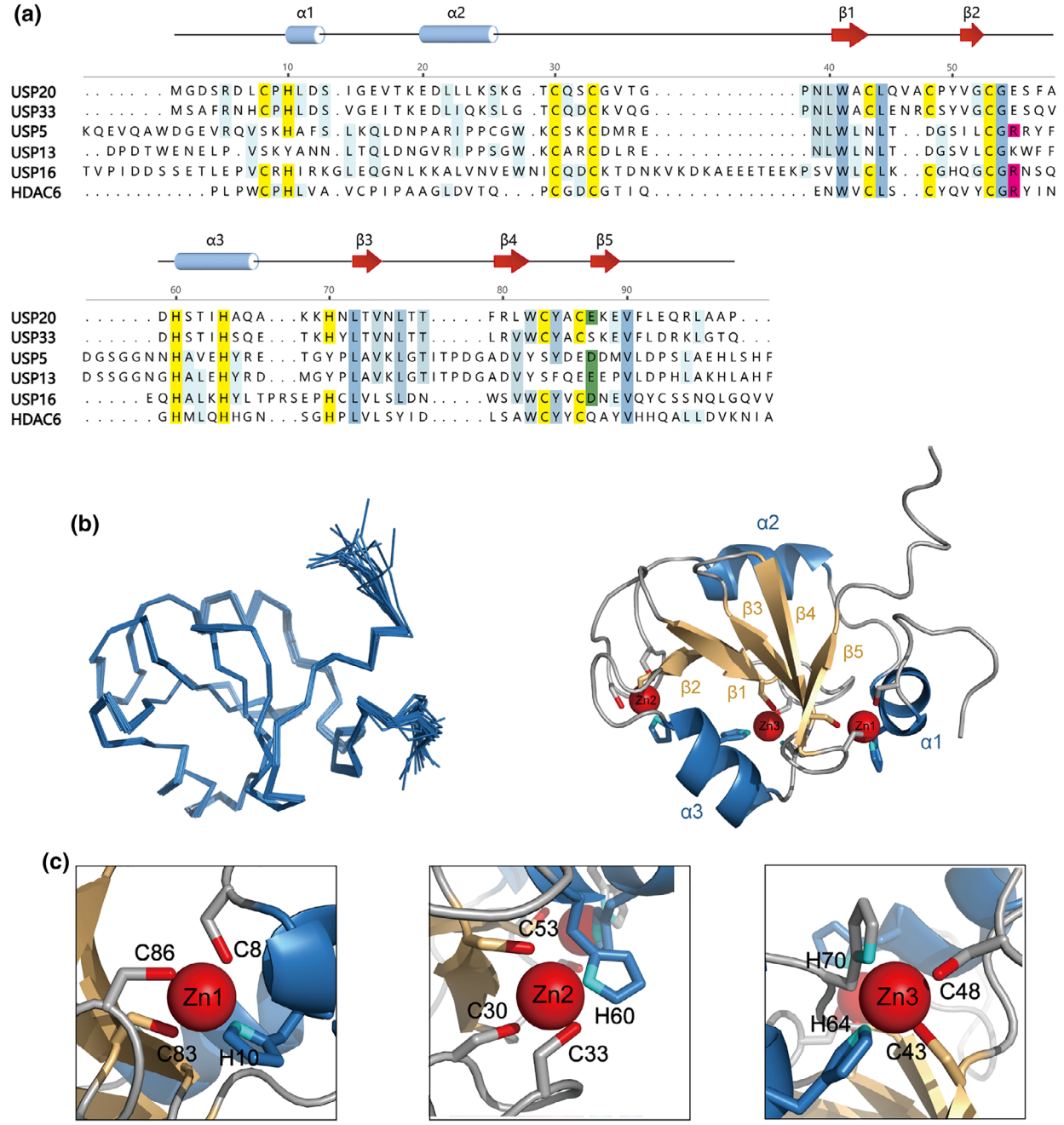

FIGURE 1 USP20 ZnF-UBP domain is well structured. (a) Sequence alignment of representative ZnF-UBP domains. Conserved residues are marked in blue, green, and red. Residues involved in zinc binding are highlighted in yellow. (b) (Left) Structural ensemble of 20 best structures of USP20 ZnF-UBP domain; (right) ribbon representation of the lowest-energy structure of USP20 ZnF-UBP domain. (c) Zoomed view of the local structures for three chelated zinc ions in USP20 ZnF-UBP domain. Zinc ions are depicted as spheres, and their coordinated residues are shown as sticks. ZnF-UBP, zinc-finger ubiquitin binding domain

ZnF-UBP domain is also different from that of USP33 ZnF-UBP domain (Figure 2b), which might affect ubiquitin binding. We further compared the structure of USP20 ZnF-UBP domain with those of ZnF-UBP domains from USP5, USP13, and USP16, and the overlaid structures were shown in Figure 2c. USP16 ZnF-UBP domain contains three chelated zinc ions in a similar coordinated pattern to the zinc ions in USP20 ZnF-UBP domain. Meanwhile, in comparison with USP20 ZnF-UBP domain, the loop before β1 in USP16 ZnF-UBP is longer, and an extra α-helix in the C-terminal of USP16 ZnF-UBP is accommodated. For the ZnF-UBP domains of USP5 and its homologue USP13, a long flexible loop instead of two α-helices is formed in their N-terminal regions right before the β-sheet structure. Moreover, USP5 ZnF-UBP domain contains only one coordinated zinc ion spatially connecting the loop L2A and the

loop before β1, and this only zinc ion is equivalent to the Zn2 in USP20 ZnF-UBP domain. It is worth noting that the key residue for ubiquitin binding (R221) in USP5 ZnF-UBP domain is substituted by an oppositely charged residue E55 in USP20 ZnF-UBP domain (Figure 1a).

TABLE 1 Structural statistics of the USP20 ZnF domain

Structural constraints	
Total NOE	1,731
Intra-residual	364
Sequential ($\|i-j\|=1$)	475
Medium range ($2 \le \|i-j\| \le 4$)	326
Long range ($\|i-j\|>4$)	386
Hydrogen bonds	42
Dihedral angle restraints	
Φ	69
Ψ	69
Ramachandran statistics	
Most favored region (%)	60.3
Allowed (%)	35.9
Generous (%)	3.3
Disallowed (%)	0.5
RMSD from mean structure (Å)	
Residues 5–95 (Backbone atoms)	0.22 ± 0.07
Residues 5–95 (all heavy atoms)	0.87 ± 0.10

Abbreviation: NOE, nuclear overhauser effect; ZnF, zinc-finger.

2.2 | USP20 ZnF-UBP domain presents weak binding capacity to mono-ubiquitin

According to the previously published literatures for the structure and function studies of ZnF-UBP domains, there is a high possibility that the ZnF-UBP domain of USP20 could not recognize ubiquitin.[29] To test this hypothesis, NMR titration experiments were performed by using ^{15}N-labeled USP20 ZnF-UBP domain and unlabeled mono-ubiquitin in varying molar ratios from 1:0 to 1:40 of USP20 ZnF-UBP to mono-ubiquitin. The ^{1}H-^{15}N heteronuclear single quantum coherence spectroscopy (HSQC) spectra of USP20 ZnF-UBP domain in the presence of increasing amounts of mono-ubiquitin were recorded (Figure 3a). With the addition of mono-ubiquitin, a few of NMR resonances corresponding to specific amino acid residues in USP20 ZnF-UBP domain present dose-dependent changes, which provide evidence for the binding of mono-ubiquitin to USP20 ZnF-UBP domain. The modest and unsaturated binding-induced chemical shift perturbations (CSPs) suggest that the binding affinity between USP20 ZnF-UBP domain and mono-ubiquitin is weak. It is worth noting that high concentrations of mono-ubiquitin are used in the NMR titration experiments. To check if this will cause any aggregation that may induce nonspecific interactions, NMR line width analysis for ubiquitin at different concentrations including 1.4, 2.8,

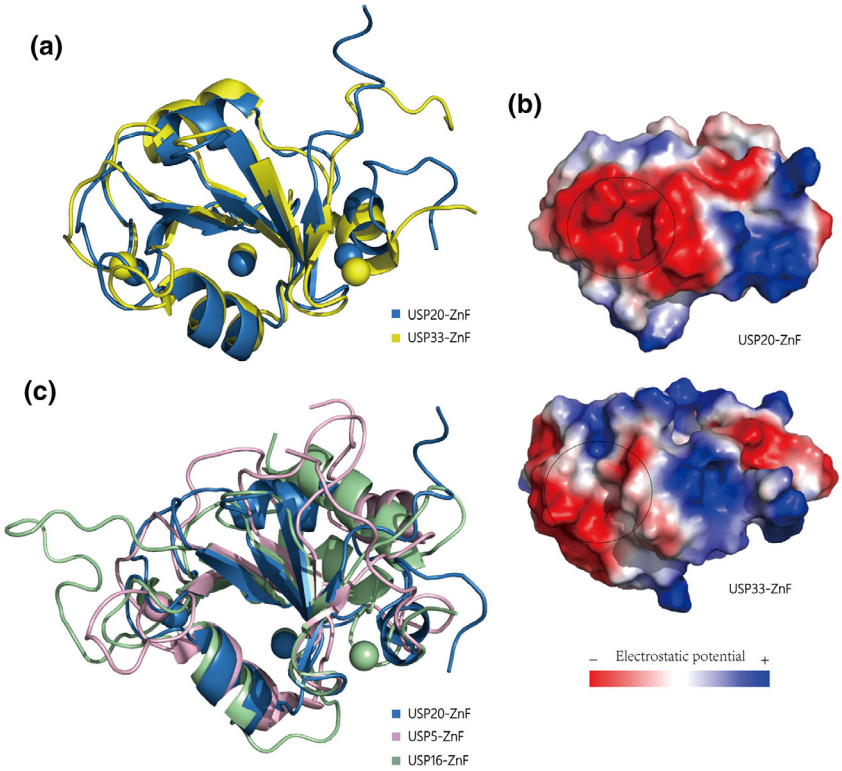

FIGURE 2 USP20 ZnF-UBP domain forms a canonical core structure essential for ubiquitin recognition. (a) Superposition of the structures for USP20 ZnF-UBP domain (blue) and USP33 ZnF-UBP domain (yellow). (b) Comparison of the electrostatic potential surfaces of USP20 ZnF-UBP domain and USP33 ZnF-UBP domain. The positive potential is shown in blue and the negative potential is highlighted in red. The canonical ubiquitin binding pocket is highlighted by black circle. (c) Structural comparison of USP20 ZnF-UBP domain (blue) with USP5 ZnF-UBP domain (pink) and USP16 ZnF-UBP domain (green). ZnF-UBP, zinc-finger ubiquitin binding domain

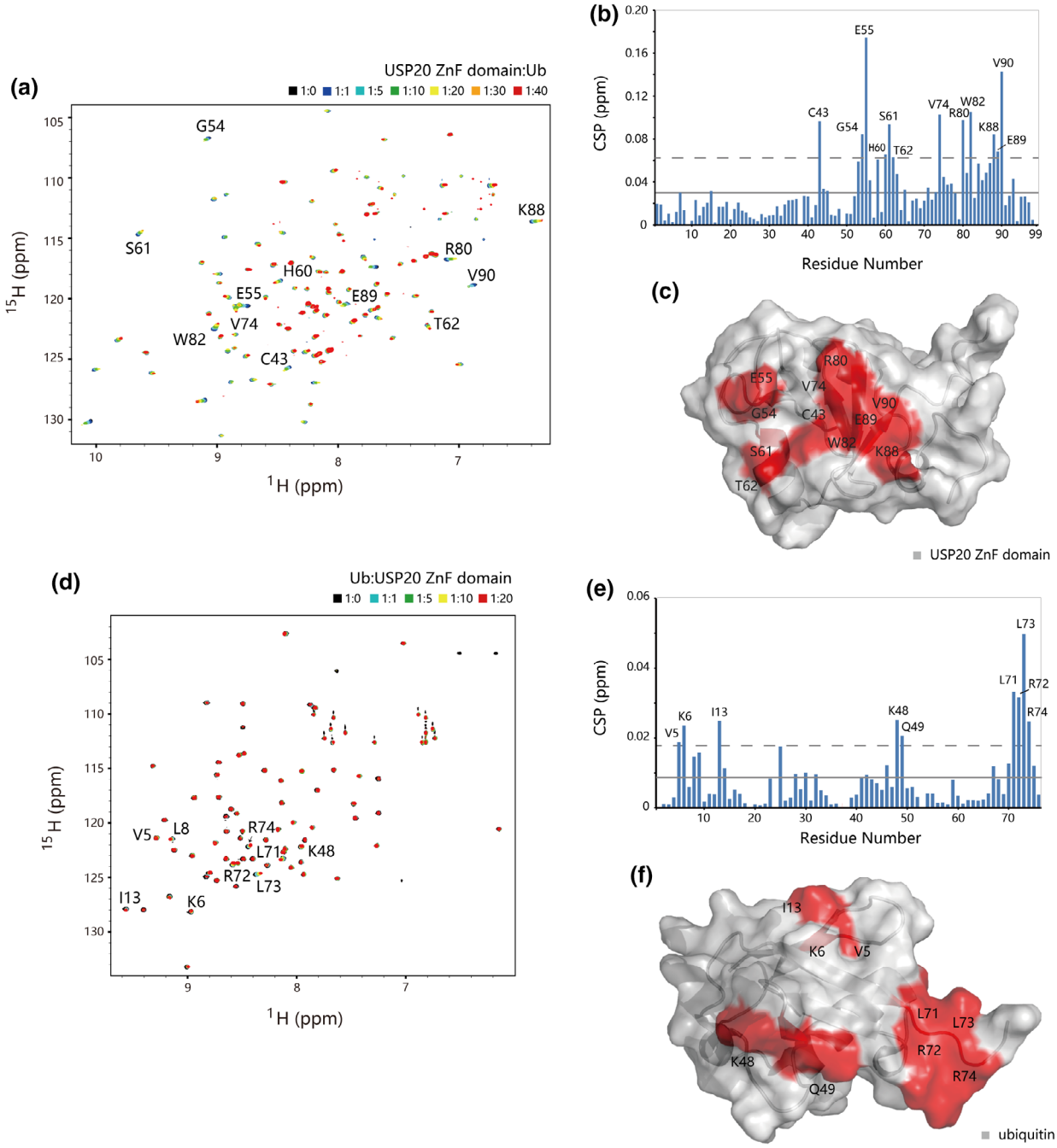

FIGURE 3 Characterization of the interactions between USP20 ZnF-UBP domain and mono-ubiquitin. (a) Superposition of the ^{1}H-^{15}N HSQC spectra of USP20 ZnF-UBP domain upon the titration of ubiquitin. The spectra are colored according to the molar ratio of USP20 ZnF-UBP domain to ubiquitin applied in spectrum acquisition: 1:0 (black), 1:1 (blue), 1:5 (sky blue), 1:10 (green), 1:20 (yellow), 1:30 (orange), and 1:40 (red). (b) Amide chemical shift perturbation analysis reveals the residues of USP20 ZnF-UBP domain involved in binding ubiquitin. The solid line and the dashed line indicate CSP average and CSP average plus standard deviation, respectively. (c) The chemical shift perturbation data of (b) is mapped onto a surface representation of USP20 ZnF-UBP. The significantly perturbed residues in USP20 ZnF-UBP are colored in red. (d) Superposition of the ^{1}H-^{15}N HSQC spectra of ubiquitin upon the titration of USP20 ZnF-UBP domain. The spectra are colored according to the molar ratio of ubiquitin to USP20 ZnF-UBP domain applied in spectrum acquisition: 1:0 (black), 1:1 (sky blue), 1:5 (green), 1:10 (yellow), and 1:20 (red). (e) Amide chemical shift perturbation analysis reveals the residues of ubiquitin involved in binding USP20 ZnF-UBP. The solid line and the dashed line indicate CSP average and CSP average plus standard deviation, respectively. (f) The chemical shift perturbation data of (e) is mapped onto a surface representation of ubiquitin. The significantly perturbed residues with their CSP values greater than CSP average plus standard deviation are colored in red. CSP, chemical shift perturbation; ZnF-UBP, zinc-finger ubiquitin binding domain

and 5.6 mM was carried out. Four representative residues of ubiquitin (V70, H68, I44, and A46) were selected according to the published literature,[32] and submitted to a further NMR line width analysis (Figure S1). No significant line width broadening and chemical shift changes were observed for all of these four residues upon the increasing of the concentration for ubiquitin, which indicates that the dominant species of ubiquitin at the highest concentration as 5.6 mM is still monomer, and therefore would not induce nonspecific interactions in the binding of ubiquitin to USP20 ZnF-UBP.

We then characterized the protein–protein interactions by calculating the CSP values and mapping the CSP data to the

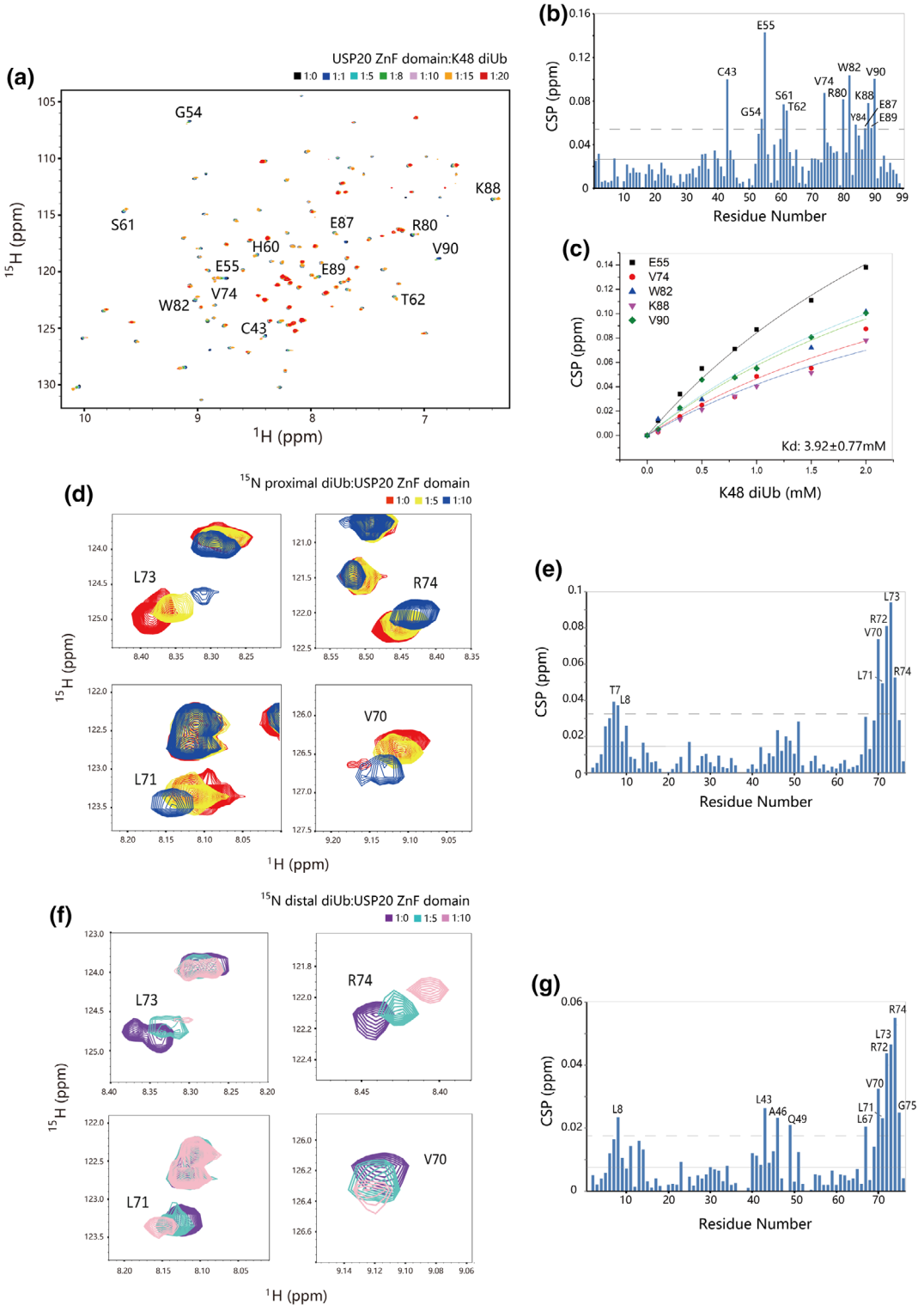

FIGURE 4 Legend on next page

solution structure of USP20 ZnF-UBP domain (Figure 3b). The CSP values for USP20 ZnF-UBP domain upon the binding of mono-ubiquitin were measured and calculated as described in Section 4. Those residues exhibiting CSP values greater than the sum of mean and standard deviation were considered as binding related residues and mapped onto the structure of USP20 ZnF-UBP domain (Figure 3c). These significantly perturbed residues are spatially clustered around the canonical hydrophobic pocket of ZnF-UBP domain, which mainly locating in the β-strands and loop L2A.

The typical binding mode of ubiquitin to ZnF-UBP domain involves its unanchored C-terminal di-glycine motif.[26] To test if this is the case in the binding of ubiquitin to USP20 ZnF-UBP domain, we performed the NMR titration experiments by recording a series of ^{1}H-^{15}N HSQC spectra of ^{15}N-labeled mono-ubiquitin in the presence of increasing amounts of unlabeled USP20 ZnF-UBP domain. In consistent with the CSP analysis data by detecting the NMR signals of ^{15}N-labeled USP20 ZnF-UBP domain, upon the addition of unlabeled USP20 ZnF-UBP protein, the NMR resonances of ^{15}N-labeled ubiquitin exhibited quite limited dose-dependent changes and were far from saturation (Figure 3d), which suggested a weak interaction between USP20 ZnF-UBP domain and mono-ubiquitin. Meanwhile, since the most perturbed residues were the C-terminal residues of ubiquitin including L71, R72, L73, and R74 (Figure 3e,f), a binding mode different from the typical C-terminal di-glycine penetration pattern for ubiquitin/ZnF-UBP domain interaction was proposed.

2.3 | Characterization of the interactions between USP20 ZnF-UBP domain and K48-linked di-ubiquitin

Mono-ubiquitination and poly-ubiquitination are associated with a variety of cellular processes. Normally, the binding affinities between ubiquitin binding domains (UBA, UIM, ZnF-UBP, etc.) and ubiquitin/poly-ubiquitin will increase upon the elongation of ubiquitin chains. Here in this article, we have demonstrated that USP20 ZnF-UBP domain exhibits a weak binding affinity to mono-ubiquitin. In addition, we then further investigated the interacting properties between USP20 ZnF-UBP domain and poly-ubiquitin (K48-linked di-ubiquitin) by synthesizing K48-linked di-ubiquitin in vitro and performing NMR titration experiments. ^{15}N-labeled USP20 ZnF-UBP domain was titrated with gradually increased K48-linked di-ubiquitin until the molar ratio of USP20 ZnF-UBP to di-ubiquitin reaching 1:20. The HSQC cross-peak changes and the calculated CSP values are shown in Figure 4a,b. The measured CSP values for five most perturbed residues (E55, V74, W82, K88, and V90) in USP20 ZnF-UBP domain with the presence of different concentrations of K48-linked di-ubiquitin were used to fit the dissociation constant (K_d) through global fitting method (Figure 4c). The obviously perturbed residues of USP20 ZnF-UBP domain by the addition of di-ubiquitin are mainly distributed in loop L2A, α3, and β-strands, which are almost identical to the results revealed by NMR titration experiments for USP20 ZnF-UBP and mono-ubiquitin system, indicating that USP20 ZnF-UBP binds to di-ubiquitin with the same interface as that used in its mono-ubiquitin recognition. Besides, comparable chemical shift changes were observed by using the mixed samples with molar ratios of 1:20 for USP20 ZnF-UBP to di-ubiquitin and 1:30 for USP20 ZnF-UBP to mono-ubiquitin, which indicating a modest increase in the binding affinity of USP20 ZnF-UBP domain to ubiquitin upon the available of additional ubiquitin subunit. To map the binding surfaces of two ubiquitin subunits in di-ubiquitin (the proximal ubiquitin and the distal ubiquitin in K48-linked di-ubiquitin) to USP20 ZnF-UBP domain, selectively ^{15}N-labeled K48-linked di-ubiquitin samples in which either di-ubiquitin's proximal or distal subunit is ^{15}N labeled were synthesized and applied to NMR titration experiments (Figure 4d–g). Upon the addition of unlabeled USP20 ZnF-UBP domain, both the proximal and the distal ubiquitin subunits of di-ubiquitin showed chemical shift changes, and the most perturbed residues clustered to the C-terminal region of ubiquitin (V70-R74). The NMR titration results demonstrate that the weak

FIGURE 4 Characterization of the interactions between USP20 ZnF-UBP domain and K48-linked di-ubiquitin. (a) Superposition of the ^{1}H-^{15}N HSQC spectra of USP20 ZnF-UBP domain upon the titration of K48-linked di-ubiquitin. The spectra are colored according to the molar ratio of USP20 ZnF-UBP domain to di-ubiquitin applied in spectrum acquisition: 1:0 (black), 1:1 (blue), 1:5 (cyan), 1:8 (green), 1:10 (purple), 1:15 (orange), and 1:20 (red). (b) Amide chemical shift perturbation analysis reveals the residues of USP20 ZnF-UBP domain involved in binding di-ubiquitin. The solid line and the dashed line indicate CSP average and CSP average plus standard deviation, respectively. (c) The dissociation constant for the binding of USP20 ZnF-UBP domain to K48-linked di-ubiquitin was determined by the global fitting analysis of CSP data. (d) ^{1}H-^{15}N HSQC spectra expanded to view representative residues in the proximal subunit of K48-linked di-ubiquitin upon the titration of USP20 ZnF-UBP domain. The spectra are colored according to the molar ratio of di-ubiquitin with its proximal subunit ^{15}N-labeled to USP20 ZnF-UBP domain applied in spectrum acquisition: 1:0 (red), 1:5 (yellow), and 1:10 (blue). (e) Amide chemical shift perturbation analysis reveals the residues of di-ubiquitin's proximal subunit involved in binding USP20 ZnF-UBP domain. (f) ^{1}H-^{15}N HSQC spectra expanded to view representative residues in the distal subunit of K48-linked di-ubiquitin upon the titration of USP20 ZnF-UBP domain. The spectra are colored according to the molar ratio of di-ubiquitin with its distal subunit ^{15}N-labeled to USP20 ZnF-UBP domain applied in spectrum acquisition: 1:0 (purple), 1:5 (cyan), and 1:10 (pink). (g) Amide chemical shift perturbation analysis reveals the residues of di-ubiquitin's distal subunit involved in binding USP20 ZnF-UBP domain. CSP, chemical shift perturbation; ZnF-UBP, zinc-finger ubiquitin binding domain

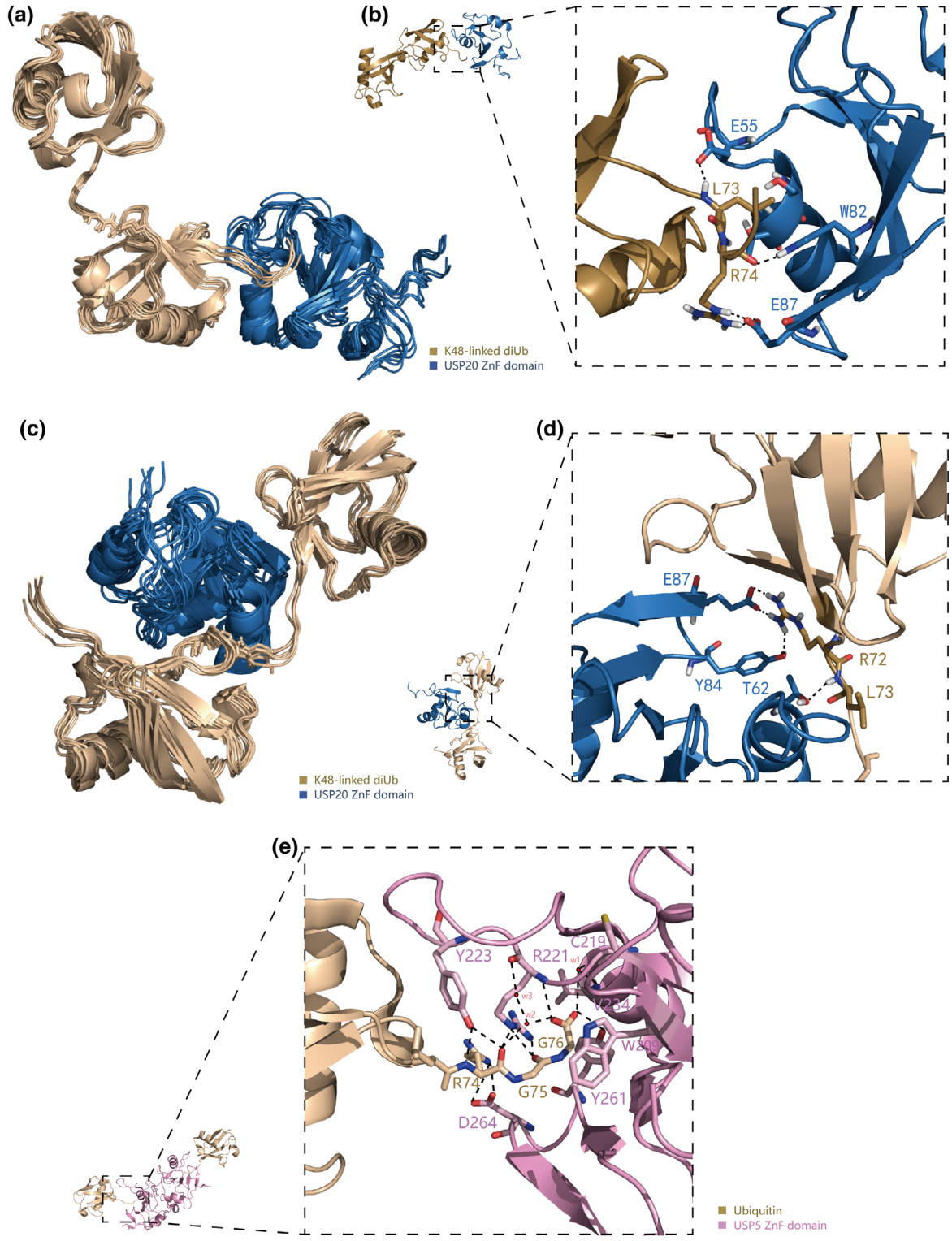

FIGURE 5 Model structures demonstrate how USP20 ZnF-UBP domain binds K48-linked di-ubiquitin. (a) Ribbon representation of the model structures for USP20 ZnF-UBP:K48-linked di-ubiquitin complex with USP20 ZnF-UBP domain (colored in blue) binding to K48-linked di-ubiquitin's proximal subunit (colored in yellow). (b) Expanded view of the USP20 ZnF-UBP:proximal ubiquitin complex reveals critical interactions. USP20 ZnF-UBP and proximal ubiquitin are highlighted in blue and yellow, respectively. (c) Ribbon representation of the model structures for USP20 ZnF-UBP: K48-linked di-ubiquitin complex with USP20 ZnF-UBP domain (colored in blue) binding to K48-linked di-ubiquitin's distal subunit (colored in yellow). (d) Expanded view of the USP20 ZnF-UBP:distal ubiquitin complex reveals critical interactions. USP20 ZnF-UBP and distal ubiquitin are highlighted in blue and yellow, respectively. (e) Expanded view of the USP5 ZnF-UBP:mono-ubiquitin complex reveals critical interactions. USP5 ZnF-UBP and mono-ubiquitin are highlighted in pink and yellow, respectively. ZnF-UBP, zinc-finger ubiquitin binding domain

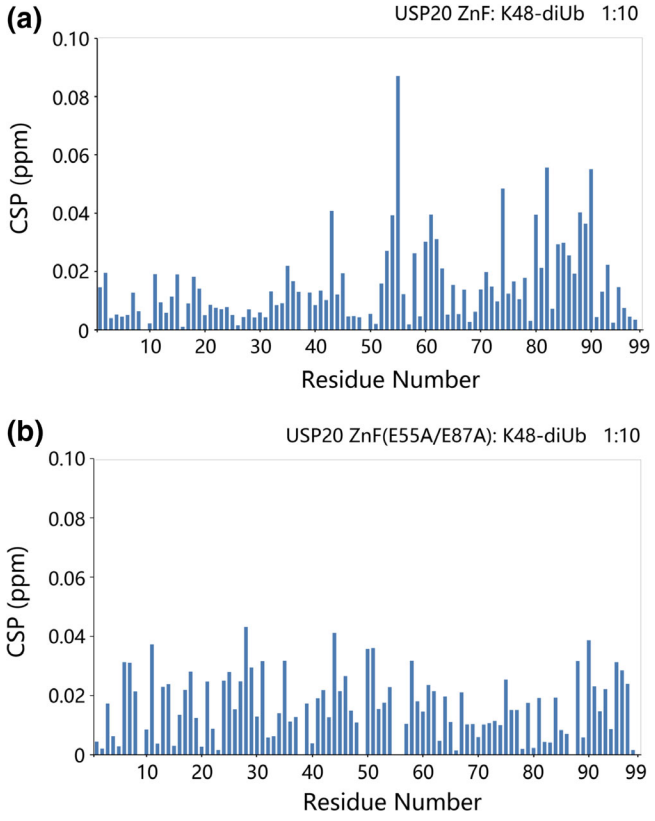

FIGURE 6 Confirmation of the binding mode between USP20 ZnF-UBP domain and K48-linked di-ubiquitin. (a) Amide chemical shift perturbation analysis data for wild-type USP20 ZnF-UBP: K48-linked di-ubiquitin system. (b) Amide chemical shift perturbation analysis data for USP20 ZnF-UBP double mutant (E55A/E87A): K48-linked di-ubiquitin system. ZnF-UBP, zinc-finger ubiquitin binding domain

interactions between USP20 ZnF-UBP domain and ubiquitin are mainly driven by the C-terminal residues (V70-R74) of ubiquitin, thereby enabling each ubiquitin subunit of di-ubiquitin to interact with USP20 ZnF-UBP domain. However, since the isopeptide bond formed between the C-terminal carboxyl group of distal ubiquitin and the K48's ε-NH_2 motif of proximal ubiquitin might hinder the binding of distal subunit in di-ubiquitin to USP20 ZnF-UBP domain due to the possible existence of steric clash, in comparison with the di-ubiquitin's proximal subunit, smaller CSPs were observed for the distal ubiquitin upon the addition of USP20 ZnF-UBP domain (Figure 4e,g).

2.4 | Models demonstrate how USP20 ZnF-UBP domain binds K48-linked di-ubiquitin

To gain more details for the interactions between K48-linked di-ubiquitin and USP20 ZnF-UBP domain, the model structures of USP20 ZnF-UBP domain complexed with K48-linked di-ubiquitin were generated by using the CSP analysis data described above and the program HADDOCK.[33] The obtained model structures for two binding modes of USP20 ZnF-UBP domain complexed with K48-linked di-ubiquitin are shown in Figure 5a–d. Both of the two cluster model structures for USP20 ZnF-UBP domain binding with either di-ubiquitin's proximal subunit or its distal ubiquitin demonstrate that the C-terminal regions of two ubiquitin subunits play crucial roles in their interactions with USP20 ZnF-UBP domain. In addition, this finding is consistent with the achieved CSP analysis results (Figure 4d–g). Although the involved key residues for two binding modes of USP20 ZnF-UBP domain to di-ubiquitin are almost identical to each other, there are distinguishable differences in the interacting patterns for the two modes. When USP20 ZnF-UBP domain interacts with di-ubiquitin's proximal subunit, multiple hydrogen bonds are formed between the paired residues from two proteins. The backbone amide group of L73 in the proximal ubiquitin forms a direct hydrogen bond with the side-chain carboxyl group of E55 in USP20 ZnF-UBP domain. The backbone carboxyl motif and side-chain guanidino group of R74 in the proximal ubiquitin form a hydrogen bond with the indole ring of USP20 ZnF-UBP's W82 and two hydrogen bonds with the side-chain carboxyl group of USP20 ZnF-UBP's E87, respectively. Besides the hydrogen bonds, R74 of proximal ubiquitin is also involved in hydrophobic contacts with USP20 ZnF-UBP's S61/T62 (Figure 5b). When USP20 ZnF-UBP domain interacts with di-ubiquitin's distal ubiquitin, the major driving force for the interactions between two proteins is from the extensive hydrophobic contacts formed between the C-terminal residues of di-ubiquitin's distal subunit and USP20 ZnF-UBP's loop L2A and α3. Moreover, R72 and L73 of distal ubiquitin are also involved in the formation of hydrogen bonds with USP20 ZnF-UBP domain (Figure 5d).

As aforementioned, the negatively charged residues (E55 and E87) in USP20 ZnF-UBP play important roles upon its interactions with ubiquitin. In addition, this is consistent with the finding that the identified binding site residues of ubiquitin are mainly positively charged (Figure 3f). However, it should be mentioned that the positively charged residues including R80 and K88 of USP20 ZnF-UBP also show significant CSPs upon the addition of ubiquitin, but they present no direct contacts with ubiquitin in the complex models. In addition, we then conclude that the chemical shift changes of these two residues (R80 and K88) are mainly induced by the consequential conformational changes instead of the direct contacts with the ubiquitin.

To confirm the generated complex models, a further mutagenesis study was conducted. USP20 ZnF-UBP E55A/E87A double mutant was created according to the CSP analysis data and the determined complex models. ^{1}H-^{15}N HSQC spectra of ^{15}N-labeled USP20 ZnF-UBP E55A/E87A double mutant without or with the presence of 10 molar excess of unlabeled di-ubiquitin were then recorded. In comparison with the wild type USP20 ZnF-UBP:di-ubiquitin system, the mutated USP20

ZnF-UBP protein presents a flattened CSP profile upon the addition of di-ubiquitin (Figure 6 and Figure S2), which indicating that the mutation of E55 and E87 abolishes the specific interactions between USP20 ZnF-UBP and K48-linked di-ubiquitin. This data confirm that the CSP analysis data and the docking models work well for identifying the key residues in USP20 ZnF-UBP responsible for ubiquitin binding.

3 | DISCUSSION

By a combination use of NMR and molecular modeling approaches, we determined the solution structure of USP20 ZnF-UBP domain, and revealed the molecular basis for the weak binding of USP20 ZnF-UBP domain to mono-ubiquitin and poly-ubiquitin. The solution structure of USP20 ZnF-UBP domain consists of a central β-sheet with either one α-helix or two α-helices packed on each side of the sheet (Figure 1b). The overall structure of USP20 ZnF-UBP domain is stabilized by three coordinated zinc ions (Figure 1c). It is worth of noting that USP20 ZnF-UBP domain does form a core structure composed of β-sheet, α3, and loop L2A, which is conserved through the diverse ZnF-UBP domains including USP5 ZnF-UBP and USP16 ZnF-UBP, and so forth (Figure 2). However, although sharing a similar global folding with other ZnF-UBP domains, extremely low binding affinities to mono-ubiquitin and poly-ubiquitin (K48-linked di-ubiquitin) were observed for USP20 ZnF-UBP domain.

The structural and functional study of USP5 ZnF-UBP domain has revealed the molecular details for its interactions with ubiquitin.[28] The C-terminal residues of ubiquitin interact with residues (R221, Y261, W209, D264, etc.) locating in the hydrophobic pocket of USP5 ZnF-UBP domain by forming direct hydrogen bonds or water-mediated hydrogen bonds and van der Waals contacts (Figure 5e). Besides, F224, situating at the top of loop L2A of USP5 ZnF-UBP domain contacts with L8 and I36 of ubiquitin through hydrophobic interactions. Consequently, the comprehensive interaction forces stabilize the ubiquitin binding orientation and strengthen the binding affinity between USP5 ZnF-UBP and ubiquitin. The corresponding residues to W209, R221, Y261, and D264 of USP5 ZnF-UBP domain, which play important roles in its ubiquitin binding, are either conserved (W41 for W209, Y84 for Y261, and E87 for D264) or substituted (E55 for R221) in USP20 ZnF-UBP domain (Figures 1 and 5). It indicates that the replacement of R221 to E55 in USP20 ZnF-UBP domain significantly demotes its interactions with the free C-terminal di-glycine motif of ubiquitin. The one residue substitution blocks the penetration of the ubiquitin's C-terminal di-glycine motif into the free C-tail recognition pocket in ZnF-UBP domain, which consequently abolishes the interactions between the other conserved paired residues in ZnF-UBP domain and ubiquitin (Figure 5). Although the electrostatic interactions between D264 (E87 in USP20 ZnF-UBP) and R74 of ubiquitin are kept (Figure 5), a significant decrease in the binding affinity of ubiquitin to USP20 ZnF-UBP domain was still observed due to the loss of the extensive interactions between ubiquitin's di-glycine motif and USP20 ZnF-UBP domain. Meanwhile, since the L2A loop in USP20 ZnF-UBP domain is shorter than that of USP5 ZnF-UBP domain, the hydrophobic interactions between the L2A loop and the residues of L8 and I36 in ubiquitin are also weakened. The sequential and structural distinctions between USP20 ZnF-UBP domain and USP5 ZnF-UBP domain greatly decrease the USP20 ZnF-UBP/ubiquitin binding affinity. Consistent with the findings mentioned above, those ZnF-UBP domains (HDAC6, USP16, etc.), which contain the conserved Arginine residue, show high binding affinities to ubiquitin with the Kds ranging from 60 nM to 6 μM.[28,34,35] While, the ZnF-UBP domains that accommodate substitution at the conserved Arginine position would show no binding to ubiquitin (Ubp8, USP33, etc.).[29,36,37] The dramatic binding affinity change caused by the replacement of a single residue suggests that the intermolecular interactions between the particular Arginine in ZnF-UBP's loop L2A and ubiquitin's C-terminal G75/G76 play a central role in the specific recognition of ubiquitin by ZnF-UBP domains.

The dramatic difference in the ubiquitin binding capacity of USP20 ZnF-UBP domain to those of other ZnF-UBP domains suggests that USP20 ZnF-UBP might have a different physiological role. In the case of USP5, its N-terminal ZnF-UBP domain binds to the C-terminus of unmodified ubiquitin, which leads to an activation of the hydrolysis activity of the enzyme. The activation effect takes place on the premise of the USP5 ZnF-UBP's high ubiquitin binding affinity, suggesting that USP20 might fail to be activated by free ubiquitin. Therefore, it is unclear whether the USP20 ZnF-UBP's ubiquitin binding capacity is too weak to be physiological significant in the ubiquitin associated system. The function of USP20 ZnF domain remains unclear and needs to be further explored. In an attempt to identify the potential substrates of USP20 ZnF-UBP domain, we carried out NMR titration experiments to detect the interactions between USP20 ZnF-UBP domain and different ubiquitin chain linkage or ubiquitin-like folds. According to the data shown in Figures 3–5, USP20 ZnF-UBP domain recognizes and interacts with the ubiquitin C-tail residues. Therefore, there is a very small possibility that USP20 ZnF-UBP domain would present binding selectivity to ubiquitin chains in different linkage. However, to test the selectivity of USP20 ZnF-UBP over ubiquitin linkages anyway, we titrated USP20 ZnF-UBP domain with M1-linked di-ubiquitin. The CSP analysis data show that compared with the binding of K48-linked di-ubiquitin to USP20 ZnF-UBP, M1-diUb interacts with USP20 ZnF-UBP domain in a similar pattern and a

comparable binding affinity (Figure S3). In the following study, we further tested the binding capacities of USP20 ZnF-UBP domain to the other two ubiquitin-like fold proteins: NEDD8 and UBL domain from hHR23A. It is revealed by the CSP analysis data that USP20 ZnF-UBP could also interact with these two ubiquitin-like proteins with comparable binding affinities to USP20 ZnF-UBP:mono-ubiquitin system (Figure S4). Overall, the obtained NMR data suggest that none of the tested proteins is the substrate of USP20 ZnF-UBP domain. Additionally, since no SUMO interacting motif exists in USP20 ZnF-UBP domain, and also the C-tail region of SUMO molecules are mainly negatively charged, the interacting capabilities between USP20 ZnF-UBP and SUMO molecules are extremely small and were not tested.

Moreover, the results of Ub-AMC hydrolysis and K48-linked di-ubiquitin hydrolysis experiments (data not shown) indicate that USP20 presents a much weaker enzymatic (deubiquitination) activity than other USPs in vitro. There is a substantial chance that the full display of the enzymatic activity of USP20 could only be induced in cellular context. In addition, it is also possible that the USP20 ZnF-UBP domain is involved in the constitution of functional protein complex, and regulate the enzymatic activity related biological processes as the ZnF-UBP domain in Ubp8 does.[36]

4 | METHODS AND MATERIALS

4.1 | Protein expression and purification

The sequence corresponding to the N-terminal ZnF-UBP domain (residues spanning 1–99) from human USP20 was amplified by PCR polymerase chain reaction (PCR) and subcloned into pET28a expression vector. The genes for UB/UB-K48R (ubiquitin/ubiquitin-K48R), E1, E2-25K, and UCH-L3 were cloned into pET-3a, pET-28a, pET-MG, and pET-22b expression vectors, respectively. The genes for M1-linked di-ubiquitin, NEDD8, UBL domain (1–82) from hHR23A, were cloned into pET-28a expression vector. The mutant for USP20 ZnF-UBP domain (E55A/E87A) was created by PCR. The expression and purification of ^{15}N and/or ^{13}C labeled USP20 ZnF-UBP domain were carried out by following the previously reported protocols.[38] Unlabeled proteins were produced by transforming the corresponding plasmids into *Escherichia coli* BL21 cells and expressed in Luria-Bertani medium. Histidine-tagged proteins were purified by a combination use of immobilized metal-ion affinity chromatography (Ni-NTA column) and size-exclusion chromatography (Superdex 75 or Superdex 200 column). The N-terminal His-tag of USP20 ZnF-UBP domain, M1-linked di-ubiquitin, UBL domain from hHR23A and NEDD8 were removed by thrombin and the C-terminal His-tags of UB/diUb (ubiquitin/di-ubiquitin) were cleaved by UCH-L3.

4.2 | NMR spectroscopy

All NMR experiments were performed at 25°C on a Bruker 600 MHz NMR spectrometer equipped with a TCI cryoprobe. ^{15}N-, ^{13}C-, and $^{15}N/^{13}C$-labeled USP20 ZnF-UBP protein samples prepared for solution structure determination were concentrated to 0.6–0.8 mM in sodium phosphate buffer containing 20 mM NaH_2PO_4/Na_2HPO_4, 100 mM NaCl, 50 μM $ZnSO_4$, 2 mM DTT, 10 or 100% D_2O (pH 6.5). Backbone and side-chain resonance assignments were completed using ^{1}H-^{15}N HSQC, HNCA, HN(CO)CA, HNCO, HN(CA)CO, HNCACB, CBCA(CO)NH, HBHA(CO)NH, H(CC)(CO)NH, (H)CC(CO)NH, and HCCH-TOCSY spectra. The backbone resonance assignments were fully achieved except for proline residues and 95% of the side-chain atoms were assigned excluding those aromatic side-chain atoms. The nuclear overhauser effect (NOE) distance restraints were derived from 3D ^{15}N-NOESY-HSQC and ^{13}C-NOESY-HSQC spectra. NMR data were processed through NMRPipe program[39] and analyzed with CARA.[40]

4.3 | Structure calculation

NOE distance restraints were derived from integral values of NOE cross-peaks, and divided into four categories (1.8–3.0, 1.8–3.6, 1.8–5, and 1.8–6 Å). Hydrogen bonding restraints were obtained from chemical shift index data and inter-strand NOEs. Backbone dihedral angle restraints (ϕ/ψ) were generated by TALOS+, using the chemical shifts of C, CA, CB, N, and HN of the corresponding residues.[41] The NOE distance restraints, torsion angle restraints, and hydrogen bond restraints were then input to calculate an ensemble of structures for USP20 ZnF-UBP domain through simulated annealing algorithm. The 20 lowest-energy structures were selected to represent the structure of USP20 ZnF-UBP domain, and the structure statistics were evaluated by the PROCHECK program.[42–44] The atomic coordinates of the determined solution structure of USP20 ZnF-UBP domain have been deposited in Protein Data Bank, and the ID code is 6KCZ.

4.4 | NMR titration experiments, CSP analysis, and NMR line width analysis

NMR titration experiments were conducted at 25°C on Bruker 600 MHz NMR spectrometers. The titration concentration of ^{15}N-labeled USP20 ZnF-UBP domain was 0.1/0.14 mM, and the concentrations of ^{15}N-UB/^{15}N-diUb were 0.1 mM. The concentrations of ^{15}N-labeled ubiquitin used in the data acquisitions of the NMR line width analysis are 1.4, 2.8, and 5.6 mM, respectively. A series of ^{1}H-^{15}N HSQC spectra were

collected after the addition of increasing amounts of unlabeled binding proteins. The spectra were processed by using NMRPipe and analyzed with Sparky.[45] CSP values ($\Delta\delta$) were derived from the geometrical distance coupled to the movement of the cross-peak and calculated using the following equation:

$$\Delta\delta = \sqrt{(\Delta\delta_N/5)^2 + \Delta\delta_H^2},$$

where $\Delta\delta_N$ and $\Delta\delta_H$ represent the observed chemical shift changes in ^{1}H dimension and ^{15}N dimension, respectively.[46] Based on the protein concentrations and the CSP values provided by the NMR titration experiments of ^{15}N-labeled USP20 ZnF and unlabeled di-ubiquitin, dissociation constant (K_d) was determined by global fitting according to the equation below:

$$\Delta\delta = \frac{\delta_{TOT}\left(nL_T + nP_T + K_d - \sqrt{(nL_T + nP_T + K_d)^2 - 4n^2L_TP_T}\right)}{2nP_T},$$

where $\Delta\delta$ donates the observed chemical shift change, d_{TOT} is the chemical shift difference between free and complexed protein, n is the binding stoichiometry, L_T is the concentration of titrant protein, and P_T is the total concentration of analyte protein.[47]

4.5 | Synthesis of K48-linked di-ubiquitin

K48-linked di-ubiquitin was synthesized by linking ubiquitin and ubiquitin-K48R in the presence of human ubiquitin-activating enzyme E1 and ubiquitin-conjugating enzyme E2-25K. These reaction materials were expressed and purified as described above. The cascade reactions were conducted in reaction buffer at 37°C for 6 hr. The product was purified by nickel affinity chromatography and size-exclusion chromatography. The purity of synthesized K48-linked di-ubiquitin was confirmed by sodium dodecyl sulfate-polyacrylamide gel electrophoresis and protein concentration was determined by UV spectrophotometry.

4.6 | NMR data-driven molecular docking

The structures of USP20 ZnF-UBP domain and K48-linked di-ubiquitin were used for complex structure calculation through the HADDOCK2.2 webserver.[33] The ambiguous interaction restraints (AIRs) were generated for the active and the passive residues defined by the CSP analysis results and the solvent accessibility data. The residues presenting significant CSP values (greater than the sum of mean and standard deviation) and being solvent accessible (with a calculated solvent accessible surface greater than 50% of the overall surface of corresponding residue) were defined as "active" and assigned AIRs. The neighbor residues of defined active residues, which might contribute to the protein–protein interactions, were recognized as passive residues. Finally, the active residues were defined as E55, T62, E87, K88 in USP20 ZnF-UBP domain, L8, R72, L73, R74 in proximal ubiquitin subunit of di-ubiquitin, and L8, A46, Q49, R72, L73, R74, G75 in distal ubiquitin subunit of di-ubiquitin. The semi-flexible residues were defined as all active and passive residues ±2 sequential residues. Thousand complex structures were calculated in the rigid-body minimization stage, and the 200 with the lowest intermolecular energy were then subjected to molecular dynamics-based refinement followed by the final refinement in explicit water. The refined structures were clustered, and the structure cluster with lowest HADDOCK score and energy was selected to represent the complex structures and analyzed by the LigPlot software.[48]

ACKNOWLEDGMENTS

This work was financially supported by the National Natural Science Foundation of China (Grant No. 21778061), and the National Science & Technology Major Project "Key New Drug Creation and Manufacturing Program" of China (Grant No. 2018ZX09711002).

ORCID

Naixia Zhang https://orcid.org/0000-0003-1509-9317

REFERENCES

1. Hershko A, Ciechanover A. The ubiquitin system. Annu Rev Biochem. 1998;67:425–479.
2. Weissman AM. Themes and variations on ubiquitylation. Nat Rev Mol Cell Biol. 2001;2:169–178.
3. Yau R, Rape M. The increasing complexity of the ubiquitin code. Nat Cel Biol. 2016;18:579–586.
4. Song L, Rape M. Reverse the curse—The role of deubiquitination in cell cycle control. Curr Opin Cell Biol. 2008;20:156–163.
5. Komander D, Clague MJ, Urbe S. Breaking the chains: Structure and function of the deubiquitinases. Nat Rev Mol Cell Biol. 2009;10:550–563.
6. Clague MJ, Barsukov I, Coulson JM, Liu H, Rigden DJ, Urbe S. Deubiquitylases from genes to organism. Physiol Rev. 2013;93:1289–1315.
7. Harrigan JA, Jacq X, Martin NM, Jackson SP. Deubiquitylating enzymes and drug discovery: Emerging opportunities. Nat Rev Drug Discovery. 2018;17:57–78.
8. Schulman BA, Harper JW. Ubiquitin-like protein activation by E1 enzymes: The apex for downstream signalling pathways. Nat Rev Mol Cell Biol. 2009;10:319–331.

9. Ye YH, Rape M. Building ubiquitin chains: E2 enzymes at work. Nat Rev Mol Cell Biol. 2009;10:755–764.
10. Buetow L, Huang DT. Structural insights into the catalysis and regulation of E3 ubiquitin ligases. Nat Rev Mol Cell Biol. 2016; 17:626–642.
11. Mevissen TET, Komander D. Mechanisms of deubiquitinase specificity and regulation. Annu Rev Biochem. 2017;86:159–192.
12. Reyes-Turcu FE, Ventii KH, Wilkinson KD. Regulation and cellular roles of ubiquitin-specific deubiquitinating enzymes. Annu Rev Biochem. 2009;78:363–397.
13. Sahtoe DD, Sixma TK. Layers of DUB regulation. Trends Biochem Sci. 2015;40:456–467.
14. Rehman SAA, Kristariyanto YA, Choi SY, et al. MINDY-1 is a member of an evolutionarily conserved and structurally distinct new family of deubiquitinating enzymes. Mol Cell. 2016;63:146–155.
15. Li ZB, Wang DK, Na X, Schoen SR, Messing EM, Wu G. Identification of a deubiquitinating enzyme subfamily as substrates of the von Hippel-Lindau tumor suppressor. Biochem Biosph Res Commun. 2002;294:700–709.
16. Curcio-Morelli C, Zavacki AM, Christofollete M, et al. Deubiquitination of type 2 iodothyronine deiodinase by von Hippel-Lindau protein-interacting deubiquitinating enzymes regulates thyroid hormone activation. J Clin Invest. 2003;112:189–196.
17. Li Z, Wang D, Messing EM, Wu G. VHL protein-interacting deubiquitinating enzyme 2 deubiquitinates and stabilizes HIF-1alpha. EMBO Rep. 2005;6:373–378.
18. Berthouze M, Venkataramanan V, Li Y, Shenoy SK. The deubiquitinases USP33 and USP20 coordinate beta2 adrenergic receptor recycling and resensitization. EMBO J. 2009;28:1684–1696.
19. Yasunaga J, Lin FC, Lu X, Jeang KT. Ubiquitin-specific peptidase 20 targets TRAF6 and human T cell leukemia virus type 1 tax to negatively regulate NF-kappaB signaling. J Virol. 2011;85:6212–6219.
20. Shanmugam I, Abbas M, Ayoub F, et al. Ubiquitin-specific peptidase 20 regulates Rad17 stability, checkpoint kinase 1 phosphorylation and DNA repair by homologous recombination. J Biol Chem. 2014;289:22739–22748.
21. Kim SR, Kim JO, Lim KH, Yun JH, Han I, Baek KH. Regulation of pyruvate kinase isozyme M2 is mediated by the ubiquitin-specific protease 20. Int J Oncol. 2015;46:2116–2124.
22. Kommaddi RP, Jean-Charles PY, Shenoy SK. Phosphorylation of the deubiquitinase USP20 by protein kinase A regulates post-endocytic trafficking of beta2 adrenergic receptors to autophagosomes during physiological stress. J Biol Chem. 2015;290:8888–8903.
23. Wu CM, Luo KT, Zhao F, et al. USP20 positively regulates tumorigenesis and chemoresistance through beta-catenin stabilization. Cell Death Differ. 2018;25:1855–1869.
24. Yu SMW, Jean-Charles PY, Abraham DM, et al. The deubiquitinase ubiquitin-specific protease 20 is a positive modulator of myocardial beta(1)-adrenergic receptor expression and signaling. J Biol Chem. 2019;294:2500–2518.
25. Hurley JH, Lee S, Prag G. Ubiquitin-binding domains. Biochem J. 2006;399:361–372.
26. Bonnet J, Romier C, Tora L, Devys D. Zinc-finger UBPs: Regulators of deubiquitylation. Trends Biochem Sci. 2008;33:369–375.
27. Searle MS, Garner TP, Strachan J, et al. Structural insights into specificity and diversity in mechanisms of ubiquitin recognition by ubiquitin-binding domains. Biochem Soc Trans. 2012;40: 404–408.
28. Reyes-Turcu FE, Horton JR, Mullally JE, Heroux A, Cheng XD, Wilkinson KD. The ubiquitin binding domain ZnFUBP recognizes the C-terminal diglycine motif of unanchored ubiquitin. Cell. 2006;124:1197–1208.
29. Allen MD, Bycroft M. The solution structure of the ZnF UBP domain of USP33/VDU1. Protein Sci. 2007;16:2072–2075.
30. Pai MT, Tzeng SR, Kovacs JJ, et al. Solution structure of the Ubp-M BUZ domain, a highly specific protein module that recognizes the C-terminal tail of free ubiquitin. J Mol Biol. 2007;370: 290–302.
31. Zhang YH, Zhou CJ, Zhou ZR, Song AX, Hu HY. Domain analysis reveals that a deubiquitinating enzyme USP13 performs non-activating catalysis for Lys63-linked polyubiquitin. PLoS One. 2011;6(12):e29362.
32. Liu Z, Zhang WP, Xing Q, Ren XF, Liu ML, Tang C. Noncovalent dimerization of ubiquitin. Angew Chem Intl Ed. 2012;51:469–472.
33. van Zundert GCP, Rodrigues JPGLM, Trellet M, et al. The HADDOCK2.2 web server: User-friendly integrative modeling of biomolecular complexes. J Mol Biol. 2016;428:720–725.
34. Boyault C, Gilquin B, Zhang Y, et al. HDAC6-p97/VCP controlled polyubiquitin chain turnover. EMBO J. 2006;25:3357–3366.
35. Ouyang H, Ali YO, Ravichandran M, et al. Protein aggregates are recruited to aggresome by histone deacetylase 6 via unanchored ubiquitin C termini. J Biol Chem. 2012;287:2317–2327.
36. Kohler A, Zimmerman E, Schneider M, Hurt E, Zheng N. Structural basis for assembly and activation of the heterotetrameric SAGA histone H2B deubiquitinase module. Cell. 2010;141:606–617.
37. Samara NL, Datta AB, Berndsen CE, et al. Structural insights into the assembly and function of the SAGA deubiquitinating module. Science. 2010;328:1025–1029.
38. Yang YY, Wen Y, Zhang NX. H-1, C-13 and N-15 backbone and side-chain resonance assignments of the ZnF-UBP domain of USP20/VDU2. Biomol NMR Assign. 2017;11:91–93.
39. Delaglio F, Grzesiek S, Vuister GW, Zhu G, Pfeifer J, Bax A. Nmrpipe—A multidimensional spectral processing system based on Unix pipes. J Biomol NMR. 1995;6:277–293.
40. Keller RLJ. The computer aided resonance assignment tutorial. Goldau: Cantina Verlag, 2004.
41. Shen Y, Delaglio F, Cornilescu G, Bax A. TALOS plus: A hybrid method for predicting protein backbone torsion angles from NMR chemical shifts. J Biomol NMR. 2009;44:213–223.
42. Laskowski RA, Macarthur MW, Moss DS, Thornton JM. Procheck—A program to check the stereochemical quality of protein structures. J Appl Cryst. 1993;26:283–291.
43. Schwieters CD, Kuszewski JJ, Tjandra N, Clore GM. The Xplor-NIH NMR molecular structure determination package. J Magn Reson. 2003;160:65–73.
44. Schwieters CD, Kuszewski JJ, Clore GM. Using Xplor-NIH for NMR molecular structure determination. Prog Nucl Magn Reson Spectrosc. 2006;48:47–62.
45. Lee W, Tonelli M, Markley JL. NMRFAM-SPARKY: Enhanced software for biomolecular NMR spectroscopy. Bioinformatics. 2015;31:1325–1327.
46. Williamson MP. Using chemical shift perturbation to characterise ligand binding. Prog Nucl Magn Reson Spectrosc. 2013;73:1–16.
47. Fielding L. NMR methods for the determination of protein-ligand dissociation constants. Prog Nucl Magn Reson Spectrosc. 2007; 51:219–242.

48. Laskowski RA, Swindells MB. LigPlot+: Multiple ligand-protein interaction diagrams for drug discovery. J Chem Inf Model. 2011; 51:2778–2786.

SUPPORTING INFORMATION

Additional supporting information may be found online in the Supporting Information section at the end of this article.

How to cite this article: Yang Y, Ding Y, Zhou C, Wen Y, Zhang N. Structural and functional studies of USP20 ZnF-UBP domain by NMR. *Protein Science*. 2019;28:1606–1619. https://doi.org/10.1002/pro.3675